HEFAT2014
10th International Conference on Heat Transfer, Fluid Mechanics and Thermodynamics
14 – 16 July 2014
Orlando, Florida

THE EFFECT OF LEADING AND TRAILING EDGE PROTUBERANCES ON AEROFOIL PERFORMANCE

Maksoud, T.M.A* and Ramasamy, V.

*Author for correspondence
School of Engineering, Faculty of Computing, Engineering and Science,
University of South Wales,
Pontypridd, Wales, CF37 1DL,
United Kingdom,
E-mail: tmaksoud@glam.ac.uk

ABSTRACT

This paper presents two-dimensional experimental and numerical studies on the aerodynamic characteristics of modified NACA 634-021 aerofoils with sinusoidal protuberances, on both the leading and trailing edges. Wind tunnel results at $Re = 2.4 \times 10^5$ showed that the standard NACA 634-021 aerofoil performed better at smaller angles of attack within its pre-stall region as compared to the wavy aerofoils with increasing protuberance amplitude. On the other hand, the wavy aerofoils were found to perform better within the baseline post-stall. The standard K-ε model using the PHOENICS CFD package revealed similar trends to those obtained from the experiments, which validated the numerical procedure. The CFD model also showed that increasing the protuberance wavelength slightly lowers the lift generated at lower angles of attack, but leads to a better performance within the baseline post-stall. Flow analysis using the K- ε model showed that in the case of the wavy aerofoils, flow separation occurs even at small angles of attack in the valleys located behind the leading edge peaks. The numerical analysis also showed that the protuberances located on the leading edge of the aerofoils act as vortex generators. The strength of the vortices increase with angle of attack and flow is energised and pulled over the leading edge peaks, which explains the stall delay characteristics of the wavy aerofoils.

INTRODUCTION

Nature can provide some guidance in the improvement of engineering applications. The transition from nature to technology is difficult to accomplish, due to the fact that biological species are flexible and slow as opposed to most engineering applications which are fast and consist of rigid bodies. For example, aircrafts fly at higher speed than birds and are much heavier. As such, mimicking the exact morphology of birds in building aircrafts would be inappropriate. A common ground however can be found in the flipper of the humpback whale, whose size overlaps some engineering applications and operates at a similar Reynolds number.

The potential benefits of tubercles on the aerodynamic performance of a wing aerofoil first came into light in the early 1990s. It was suggested that the tubercles reduce drag [1], while it was theorized that the morphology and placement of the leading edge tubercles act as enhanced lift devices that control the flow around the flipper. This maintains lift at high angles of attack, therefore delaying the stall [2]. Numerical investigation was performed to determine the influence of leading edge tubercles on wing performance [3]. Two rectangular wing sections were modelled, one of which had tubercles on its leading edge. The analysis of the lift and drag forces at an angle of attack of ten degrees ($\alpha = 10°$) showed a 4.8% increase in lift, a 10.9% reduction in induced drag and a 17.6% increase in lift-to-drag ratio for the wing with tubercles, versus the same wing without tubercles.

Flow around the flipper of the humpback whale was experimentally examined, [4], whereby two scale models of the pectoral flipper were designed; one which included leading edge tubercles, while the other had a smooth leading edge used for comparison. Wind tunnel experiments showed that the presence of tubercles increased the maximum lift coefficient by 6% and delayed stall angle by 40%. Overall, the scalloped model fared better at higher angles of attack. The purpose of the tubercles were compared to that of the vortex generators which energize the flow and keep the flow attached to the surface, despite the adverse pressure gradient, thus maintaining and increasing lift even at higher angles of attack, whereby stall normally occurs. Water tunnel experiments performed at low Reynolds number, [5], showed that the presence of tubercles on the leading edge of a rectangular NACA 634021 aerofoil decreased its performance in the pre-stall regime. In the post-stall region, it was found that the lift coefficient of the aerofoils with protuberances on the leading edge had a higher lift coefficient and drag was independent of the geometry. Thus aerofoil sections with tubercles on the leading edge performed

better post-stall, due to a higher lift-to-drag ratio. Flow visualization showed that flow separation occurred mainly in the troughs; in between the protuberances and was independent of wavelength.

Controlling flow separation can lead to an increase in system performance with consequent energy conservation as well as weight and space savings. Methods involving flow separation control can be split into two categories: active and passive flow control methods. Active flow control methods involve moving parts which require a source of energy for their functioning. For example, boundary layer suction is considered as active flow control, since external energy is required in the removal of the lower part of the boundary layer, close to the solid surface. On the other hand, passive flow control methods involve no moving parts and require no external energy. Examples of passive flow control devices include stationary vortex generators and gurney flaps. Passive control schemes are less complex, require little maintenance and have no direct cost associated with them apart from the initial installation. However, with the non-moving parts in the flow field, passive flow control schemes have shown disadvantages; such as increase in drag as opposed to active mechanisms, which can be mechanically manipulated and activated at specific times.

There is therefore a need to develop better passive flow methods which would increase lift whilst lowering the drag. The tubercles which act as passive flow control devices on the leading of the flippers of the humpback whale can be used as a template in improving the performance aerofoils. While research has been carried out on the effect of protuberances on the leading edge of aerofoils, at the current time, there is no work regarding the effect of similar unevenness on both the leading and trailing edges of aerofoils.

NOMENCLATURE

C_L	[-]	coefficient of lift
C_D	[-]	coefficient of drag
D	[N]	drag generated
L	[N]	lift generated
L/D	[-]	lift-to-drag ratio
$\overline{p}$	[Pa]	mean component of pressure
$\overline{u}$	[m/sec]	mean component of velocity
α	[deg]	angle of attack
μ	[Pa sec]	dynamic viscosity
ρ	[kg/ m^3]	density of fluid

METHODOLOGY - EXPERIMENTS

The effect of protuberance amplitude of the aerofoil performance was experimentally investigated. Three wavy aerofoils with a constant wavelength of 0.25c but with varying amplitude were fabricated along the NACA 634-021 baseline aerofoil using the rapid prototype machine. The chord length and span of all the aerofoils designed were 100mm and 200mm respectively. The 3 wavy aerofoils machined consisted of protuberances of a constant wavelength of 25mm with amplitudes of 0.025c, 0.05c, 0.12c. The set of aerofoils machined are shown in Figure 1.

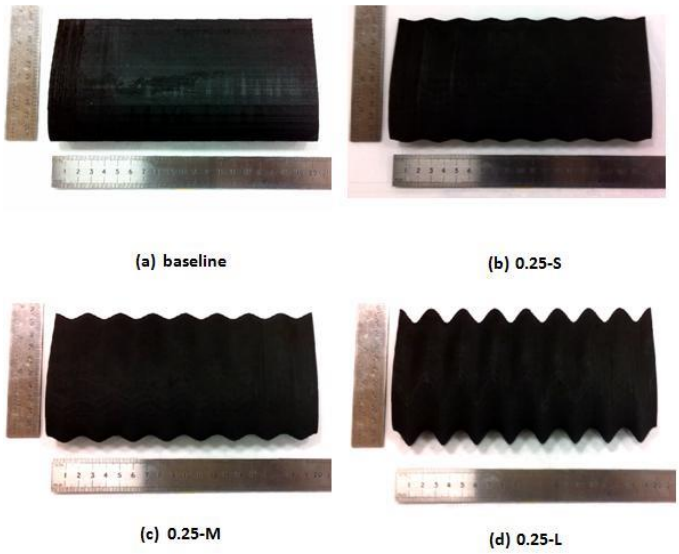

Figure 1: Fabricated aerofoils

The nomenclature used to describe the wavy aerofoils throughout this paper are as follows: amplitudes of 0.025c, 0.05c and 0.12c are respectively denoted by S (small), M (medium) and L (large), while wavelengths 0.25c, 0.5c and 1c are respectively represented by 0.25, 0.5 and 1.

The experiments were conducted in a wind tunnel. The experiments were conducted over $0° \leq \alpha \leq 25°$ at a constant Reynolds number of 2.4×10^5, based on the fluid velocity of 35m/s and a plan form area of 0.02m^2. The lift and drag forces acting on the aerofoils were measured electronically through load cells. The output from the cells was taken via an amplifier to a microprocessor-controlled display module mounted onto the wind tunnel control and instrumentation frame whereby the lift and drag were digitally displayed. The measured data were then converted to lift and drag coefficients using the plan form area and free-stream dynamic pressure.

COMPUTATIONAL METHODS

The geometry of the aerofoil bodies used for the numerical analysis were similar to those from the experiment. The effect of wavelength was also numerically investigated with aerofoils of constant protuberances amplitude of 12mm with varying wavelengths of 25mm, 50mm and 100mm. The aerofoil models with varying wavelength are shown in Figure 2.

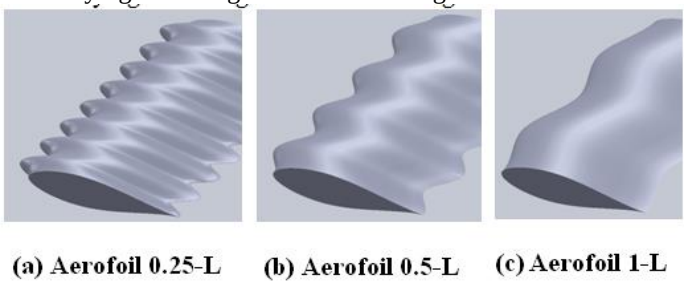

Figure 2: Aerofoils with varying wavelength

K- ε model established by Launder and Spalding (1974) was used to simulate the flow around the aerofoils for the particular

Reynolds number of 2.4×10^5. The time average continuity and the RANS equations are as follows:

$$\frac{\partial \overline{u_i}}{\partial x_i} = 0$$

$$\rho \frac{\partial \left(\overline{u_i}\,\overline{u_j}\right)}{\partial x_j} = -\frac{\partial \overline{p}}{\partial x_i} + \frac{\partial}{\partial x_j}\left(\mu \frac{\partial \overline{u_i}}{\partial x_j} - \rho \overline{u_i' u_j'}\right)$$

where i =1 and 2 respectively represent the stream-wise and vertical directions. The term $\rho\overline{u_i' u_j'}$ denotes the Reynolds stress tensor. 'Closure' is brought to the gap that exists between the greater numbers of unknowns than equations by using the eddy-viscosity concept proposed by Boussinesq. The Reynolds stress tensor - $\rho\overline{u_i' u_j'}$ is determined as follows:

$$-\rho\overline{u_i' u_j'} = v_t\left[\frac{\partial \overline{u_i}}{\partial x_j} + \frac{\partial \overline{u_j}}{\partial x_i}\right] - \frac{2}{3}\rho\delta_{ij}k$$

where k is the turbulent kinetic energy, δ_{ij} being the Kronecker delta function and v_t is the eddy viscosity. In the standard K- ε model proposed by Launder and Spalding (1974), v_t can be calculated from the following equation:

$$v_t = \frac{C_\mu k^2}{\varepsilon}$$

where C_μ is a constant of 0.09 and k and ε are the turbulent kinetic energy and turbulent kinetic energy dissipation rate respectively.

k and ε can be obtained as follows:

$$\frac{\partial(\rho\overline{u_i}k)}{\partial x_i} = \frac{\partial}{\partial x_i}\left[\frac{v_t}{\sigma_k}\frac{\partial k}{\partial x_i}\right] + P - \rho\varepsilon$$

$$\frac{\partial(\rho\overline{u_i}\varepsilon)}{\partial x_i} = \frac{\partial}{\partial x_i}\left[\frac{v_t}{\sigma_\varepsilon}\frac{\partial \varepsilon}{\partial x_i}\right] + \frac{\varepsilon}{k}(C_1 P - C_2\rho\varepsilon)$$

P represents the rate of production of turbulence kinetic energy and is obtained from the following equation:

$$P = -\rho\overline{u_i u_j}\frac{\partial U_i}{\partial x_j}$$

C_1,C_2, σ_k and σ_ε are empirical constants whose standard values are 1.45, 1.90, 1.0 and 1.3 respectively.

PHOENICS uses the finite volume method to solve the partial differential equations. The computational domain used for the analysis is shown in Figure 3.

Since a 2-dimensional analysis was performed, the size of the domain along the z-axis was made equal to the span of the aerofoil bodies, which is 200 mm. The aerofoils were placed within the domain such that the upstream inlet boundary was located 0.15c from the leading edge, while the downstream outlet boundary was located at 0.32c from the trailing edge. The lateral boundaries were located 0.13c away from the aerofoils at α = 0°. However, the distances of the lateral boundaries from the aerofoils change at different angles of attack. The size of the domain in millimetres was 550×300×200 and the domain material set to air at 20°c at 1 atm. The reference pressure was set at 1.013×10^5 Pa while the external ambient pressure was set at 0 Pa relatively for the domain outlet. At the inlet, a uniform oncoming flow of 35 m/s in the x-direction was set with a turbulence intensity of 1.5%. All results were subject to a global convergence criterion within 0.01%.

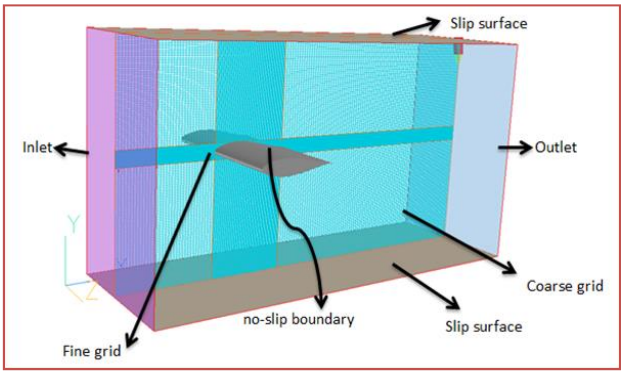

Figure 3: Computational domain

At the outlet, the external pressure was set at the ambient pressure of 0 Pa. The lateral surfaces were treated as slip surfaces, with the slide velocity in the x-direction being 35 m/s. At the surface of the aerofoils, the non-slip boundary condition was imposed.

Grid independence tests and the validation of the numerical models are vital prior to extensive simulations. The effect of grid resolution within the area enclosing the aerofoils on the aerodynamic forces was examined. It should be noted that lowering the initial cell factor, increases the resolution. The tests were conducted on the wavy aerofoil 0.25-L at angles of attack of 6° and 10° as shown in Table 1.

Initial cell factor	α	CL	CD
0.007	6°	0.5966	0.1227
0.004	6°	0.4833	0.0922
0.002	6°	0.4761	0.0955
0.001	6°	0.4735	0.0946
0.007	10°	0.8515	0.1679
0.004	10°	0.7481	0.1495
0.002	10°	0.7126	0.1425
0.001	10°	0.7254	0.1406

Table 1: Grid independence tests

The tests showed that the lift and drag coefficients at angles of attack 6° and 10° converge with increasing resolution. Doubling the resolution from an initial cell factor of 0.002 to 0.001 changes the lift and drag coefficient at α = 6° by only 0.5 % and 0.9% respectively. Similarly, changing the initial cell factor from 0.002 to 0.001 produced little change in the lift and drag coefficients at α = 10°. Thus, to save computer time, an initial cell factor of 0.002 was adopted for the rectangular area enclosing the aerofoils at all angles of attack.

To check for the accuracy of the model, the lift coefficients of aerofoil 0.25-L at angles of attack 6° and 10° obtained were compared to those from the experiment. A discrepancy of only 1.5% and 2.5% was found in between the numerical and experimental values of lift coefficients at angles of attack of 6° and 10°. This close agreement in the previous lift coefficient values indicates the accuracy and suitability of the numerical approach in predicting the flow at various angles of attack. As such, analysis of all 6 aerofoils was performed over angles of attack ranging from 0° to 25° using the standard K- ε model.

RESULTS & DISCUSSION

BASELINE AEROFOIL (EXPERIMENTAL)

The time averaged lift and drag forces experienced by the aerofoils were determined as a function of the angle of attack from the data collected from the experiments. Throughout this paper, dimensionless coefficients, such as lift and drag coefficients will be used in the description of these forces. Sources of errors in experimentation were analysed. Vibration effects were eliminated by the use of filters and load cell to measure forces indicated an global error of ±.02%.

Figure 4 shows the trend of section lift coefficient (C_L) as a function of the angle of attack (α). The lift coefficient increases at a linear rate up to α ≈ 10°, after which it keeps on increasing at a slower rate until a max C_L value of 1.1 is reached at an angle of attack of 17°. Stalling occurs with further increases in the angle of attack, as the flow separation occurs along the entire upper surface of the aerofoil.

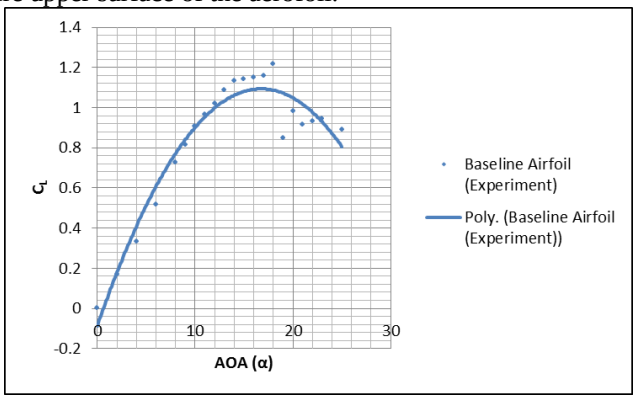

Figure 4: Lift coefficient v/s angle of attack (baseline aerofoil)

The drag coefficient (C_D) of the baseline aerofoil is lower at lower angles of attack when the area projected by the aerofoil is at its minimum. As the angle of attack is increased, the drag coefficient also increases in a quadratic fashion until a sudden increase in drag is noted whenever stall occurred. The minimum drag coefficient obtained is 0.039 at α = 0°, while the maximum CD value occurred at α = 25°.

Figure 5 shows the trend of drag coefficient of the baseline aerofoil as function of the angle of attack. Figure 6 shows the trend of the lift-to-drag ratio as a function of the angle of attack. The L/D of the aerofoil increases with increasing α ranging between 0° – 11°, with the maximum L/D value being 10 at α = 11°. Any further increase in the angle of attack subsequently decreases the lift-to-drag ratio.

BASELINE AEROFOIL (K- ε MODEL V/S EXPERIMENTAL)

Figure 7 shows the lift curve comparison of the baseline aerofoil obtained from the K- ε model to that from the experiment. It can be clearly seen that the results from the K- ε model are the same for α ≤ 13°, after which the lift curve of the K- ε model slightly deviates from the one obtained from the experiment. The maximum lift coefficient obtained from the K- ε model is 1.12 at α = 18°, as opposed to that of the experiment which shows a maximum C_L of 1.1 at α = 17°.

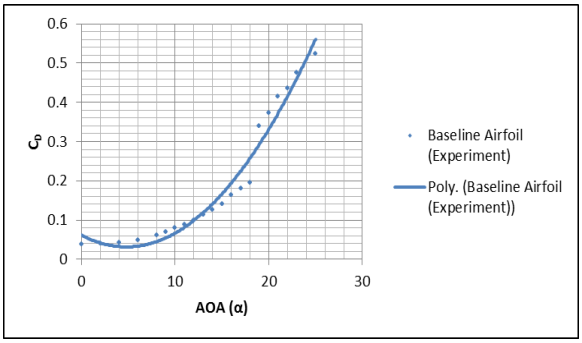

Figure 5: Drag coefficient v/s angle of attack (baseline aerofoil)

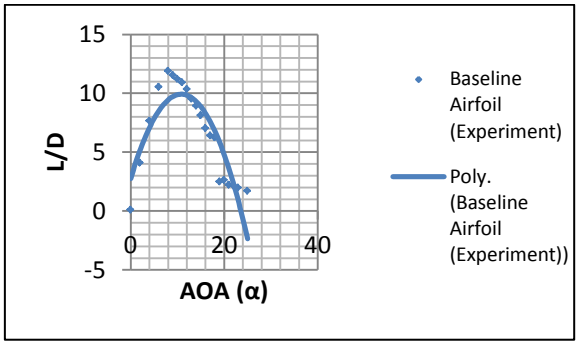

Figure 6: Lift-to-drag ratio v/s angle of attack (baseline aerofoil)

Comparison of the K- ε drag curve to that of the experiment, showed that the K- ε model overestimates the drag when 0° ≤ α ≤ 16° and underestimates its value for 18° ≤ α ≤ 25°. The drag overestimation is as much as 100 % at α = 6° when the C_D value according to the K- ε model is 0.08, as opposed to 0.04 obtained from the experiment. The K- ε model drag curve does however show the increasing drag behaviour expected with increasing α.

Figure 8 shows the comparison of drag curves as a function of the angle of attack obtained from the experiment and the K- ε model. As result of the large differences in the drag coefficients from the K- ε model and experiment, the lift-to-drag ratio curves as shown in Figure 9 also show discrepancies. Overall, the K- ε model shows great accuracy in determining the lift, while large discrepancies occurred in determining the drag, which ultimately affected the lift-to-drag ratio. In spite of those differences, the K- ε model does provide the adequate shape for a curve involving CD and L/D with respect to α.

Thus combined with the accurate lift curve obtained using the K- ε model, it can be concluded that the latter can be used as a tool in the parametric study of the wavy aerofoils.

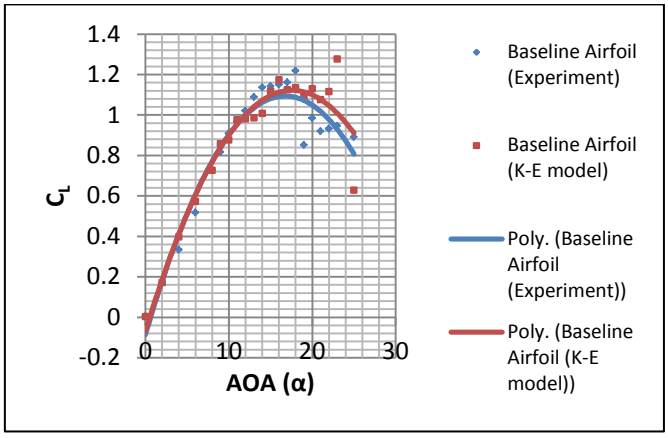

Figure 7: Lift curve comparison (baseline aerofoil)

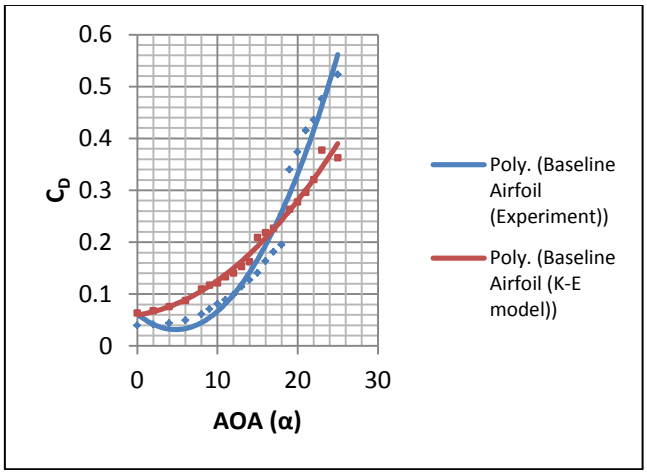

Figure 8: Drag curve comparison (baseline aerofoil)

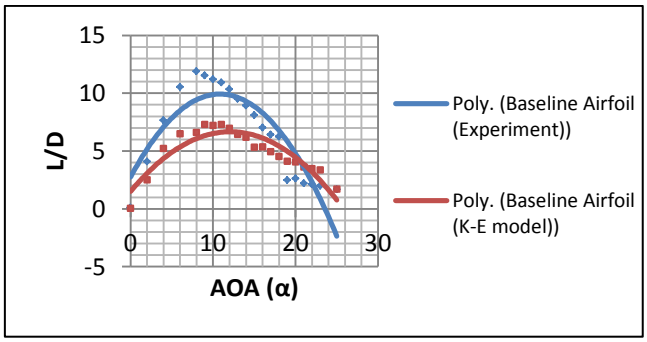

Figure 9: L/D curve comparison (baseline aerofoil)

Figure 10, shows the two-dimensional contours of the velocity in the vertical X-Y plane, around the baseline aerofoil at selected angles of attack. It can be clearly observed that the flow separation develops from the trailing edge, starting when α =10°, which is consequently the angle of attack at which the break in the linear relationship between the lift coefficient and α was observed. The separated region gradually develops on the upper surface of the aerofoil, from the trailing edge upstream towards the leading edge with an increasing angle of attack, which eventually leads to stall. The trailing-edge stall behaviour exhibited by the baseline aerofoil at high angles of attack is consistent with the characteristic of aerofoils with high thickness-to-chord ratio (above 16%).

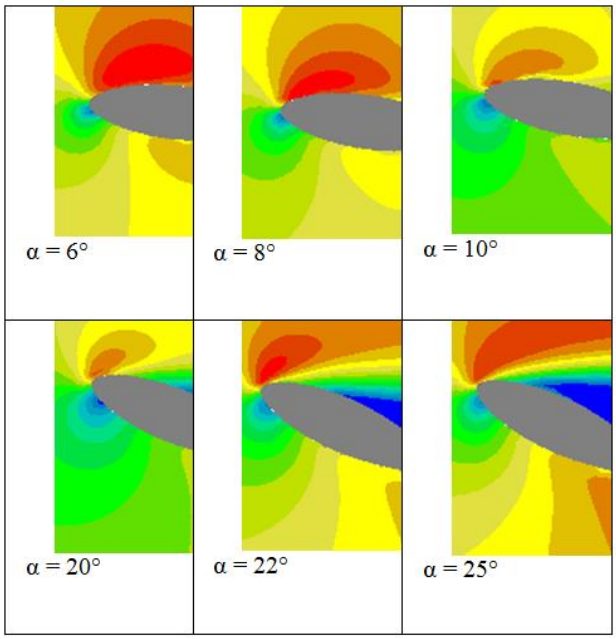

Figure 10: Velocity contours at various angles of attack (baseline aerofoil)

EFFECT OF AMPLITUDE

The effect of the amplitude of the protuberances at a fixed wavelength of 0.25c on the lift coefficient of the aerofoil is shown in Figure 11, which includes both the experiment and the K- ε model lift curves.

Results obtained from the experiment show that increasing the amplitude of protuberances, drifts the respective lift curves away from that of the baseline lift curve, thus lowering the lift coefficient in baseline pre-stall regime. Aerofoil 0.25-S has a lower lift coefficient than the baseline aerofoil up to 16°, whilst for aerofoils 0.25-M and 0.25-L, they have a lower lift coefficient than the baseline aerofoil up to 18° and 20° respectively.

The wavy aerofoils show better lift performance at higher angles of attack, thus further delaying stall with increasing amplitude. In addition, as shown in Figure 11, stall intensity decreases with increasing amplitude. The maximum lift coefficient of the 0.25-S aerofoil is found to be slightly higher than that of the baseline aerofoil and it occurs at a higher angle of attack.

Increasing amplitude of the waves on the aerofoil also lowers the maximum lift coefficient with aerofoils 0.25-S, 0.25-M and 0.25-L, having a maximum lift coefficient of 1.12, 1.08 and 1.04 respectively. The lift curves of aerofoils 0.25-S and 0.25-M are basically similar, while that of the 0.25-L aerofoil further drifts away. This can be explained by the fact that a much larger difference in the amplitude of the protuberances exists between the aerofoils 0.25-S and 0.25-L (95mm), as opposed to that of 0.25-S and 0.25-M (25mm).

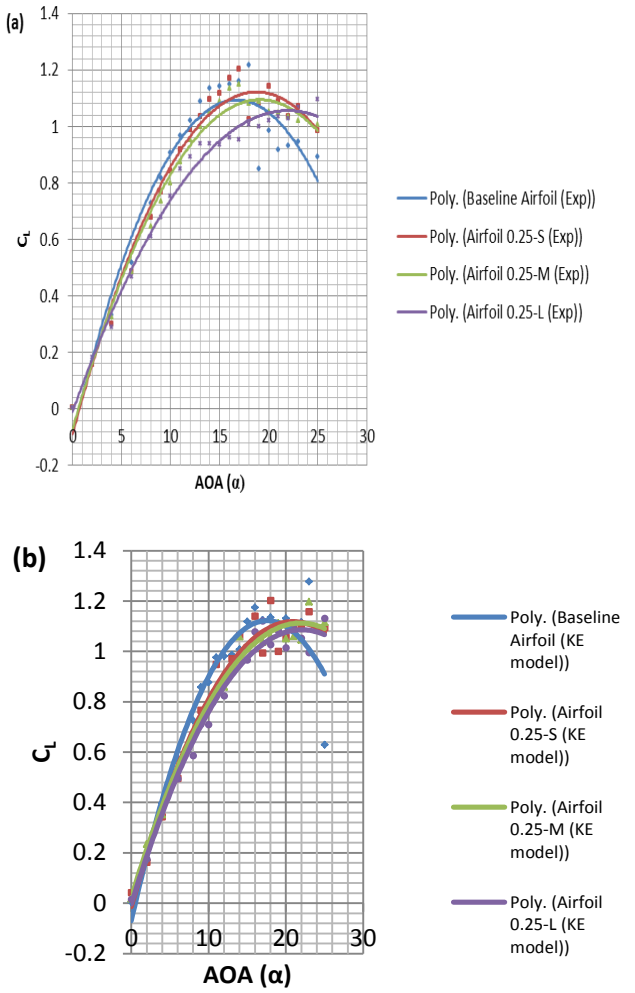

Figure 11: Effect of amplitude on lift: (a) experiment, (b) K-E model

Results obtained from the K- ε model, show similarity to those obtained from the experiment, with minor discrepancies. The similarities include:

- prediction of the stall delay of the wavy aerofoils
- better performance of the wavy aerofoils at larger angles of attack
- a lower lift coefficient in the baseline pre-stall regime with increasing protuberance amplitude
- decreasing maximum lift coefficient with increasing protuberance amplitude
- Stall delay with increasing protuberances amplitude

K- ε Modelling showed similar stall intensity irrespective of amplitude, in contrast to the experiment which shows that increasing the amplitude decreases the stall intensity. In addition, the lift curve of the 0.25-L aerofoil obtained from the CFD analysis is closer to those of the 0.25-S and 0.25-M aerofoils when compared to the experimental lift curves.

Figure 12 shows the effect of the amplitude of the protuberances on the drag from both the experiment and K- ε model.

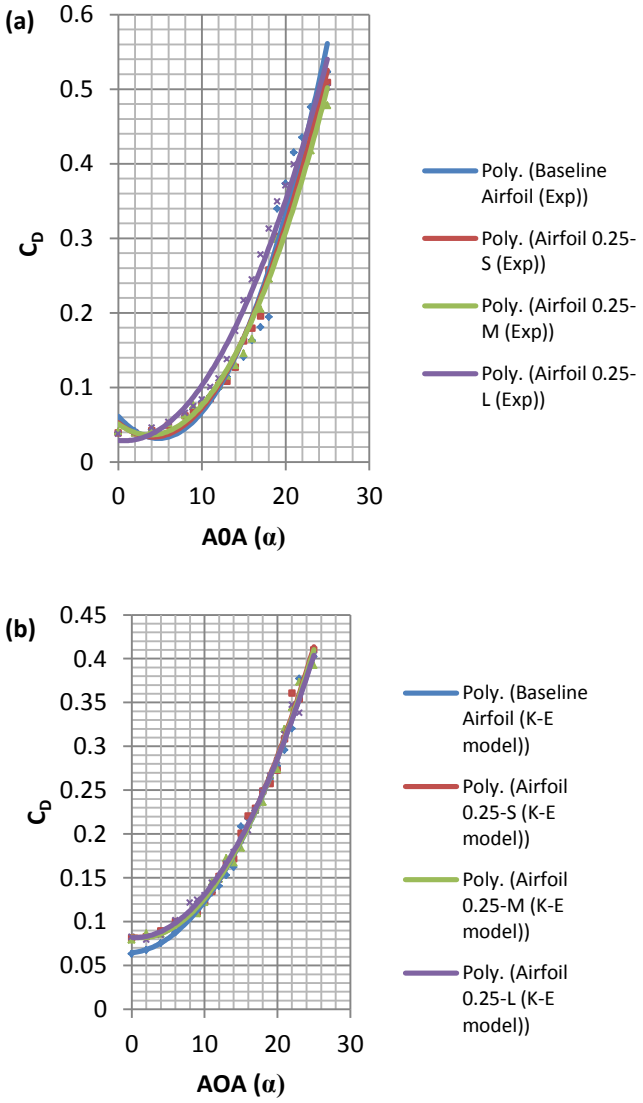

Figure 12: Effect of amplitude on drag: (a) experiment, (b) K-E model

As expected, drag results from the experiment shown in Figure 12 demonstrate low drag at low angles of attack. The trend of the drag curves of the baseline aerofoil, along with aerofoils with the small and medium amplitude (0.25-S and 0.25-M) are similar over $0° \leq \alpha \leq 18°$, after which the drag curves slightly deviate from one another. The baseline aerofoil is shown to experience higher drag at higher angles of attack (> 18°), followed by aerofoils 0.25-S and 0.25-M respectively. Aerofoil 0.25-L, with the largest amplitude experiences the largest drag over $5° \leq \alpha \leq 20°$ but, eventually has lower drag coefficient in the post-stall regime of the baseline. In addition, contrary to the baseline aerofoil, all 3 wavy aerofoils do not

exhibit the large jump in drag that occurs at the stall angle due to the strong flow separation.

Similar to the drag prediction of the baseline aerofoil, K- ε modelling overestimates the drag at angles of attack ranging from 0° to 16°, while underestimating the drag with further increase in α. The drag curves for the wavy aerofoils obtained using the K- ε model show that amplitude variation does not have any effect on the drag. As shown in Figure 12, the coefficient of drag curves of aerofoils 0.25-S, 0.25-M and 0.25-L basically lay on top of each other. CFD analysis shows that the baseline aerofoil has a better drag characteristic at low angles of attack ($0° \leq \alpha \leq 8°$).

Figure 13 shows the effect of the amplitude of the protuberances on the lift-to-drag ratio, from both the experiment and K- ε model. Results from the experiment show that the presence of the waves on the aerofoil lowers the maximum lift-to-drag ratio. In addition, increasing the amplitude decreases the maximum L/D. This is expected as lower lift coefficients, along with similar and higher drag coefficients were obtained for the wavy aerofoils when compared to the baseline in its pre-stall regime. The maximum L//D for all 4 aerofoils occurs at $\alpha = 11°$. Higher L/D is achieved by the aerofoils with increasing amplitude beyond the baseline post-stall regime, which can be explained by the fact that at those particular angles of attack, the wavy aerofoils produce more lift with little or no drag penalty.

Similar trends are observed with the L/D obtained from the CFD analysis. However, the maximum lift-to-drag ratios for all 4 aerofoils are smaller than those obtained from the experiment, which is expected due to the differences in drag.

When compared to the experiment, the K- ε model shows a larger gap between the maximum L/D of the baseline to that of aerofoil 0.25-S. This can be attributed to the fact that according to the K- ε model, the baseline aerofoil has a better drag performance at similar angles of attack. In addition, as shown in Figure 13, the K- ε model show that the peaks of the L/D curves of the wavy aerofoils being closer to each other, which is due to no significant difference in drag experienced by the 3 aerofoils over the whole range of angles of attack tested.

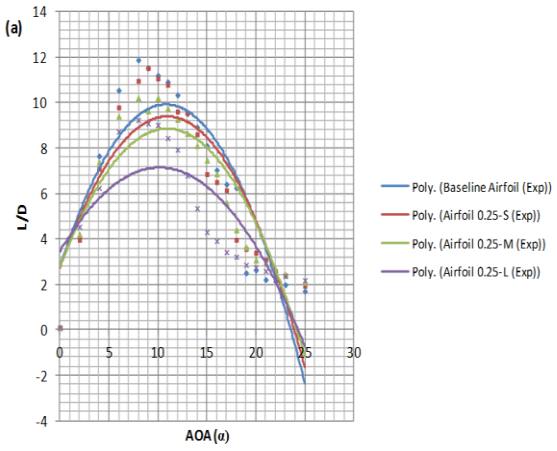

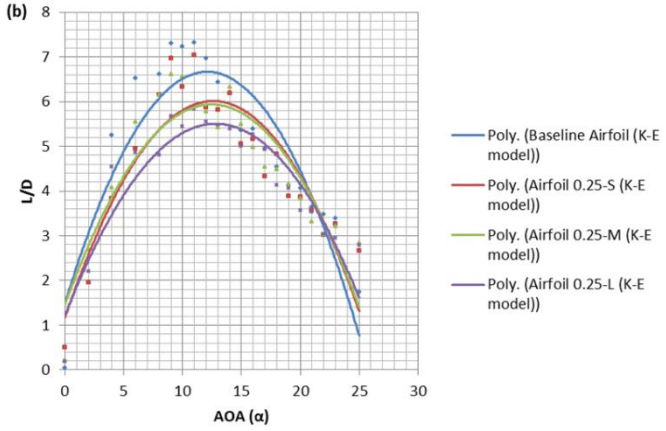

Figure 13: Effect of amplitude on L/D: (a) experiment, (b) K-E model

EFFECT OF WAVELENGTH

Even though large discrepancies occurred in drag calculation at higher AOA when compared to that of the experiment, the k- ε model showed a high degree of accuracy in predicting the effect of amplitude on the lift and drag forces in trends. Therefore, it was used as a comparison tool in determining the effect of varying protuberance wavelength at constant amplitude.

The effect of the wavelength of the protuberances at fixed amplitude of 0.12c on the lift performance of the aerofoil at various angles of attack was determined, using the K- ε model and is shown in Figure 14.

Aerofoil 1-L which has the largest wavelength is found to have the least lift performance within the baseline pre-stall regime. No significant difference is found in lift performance of aerofoils 0.25-L and 0.5-L, at lower angles of attack which may be due to the fact of the smaller difference in wavelength between the 2 aerofoils, which is only 25 mm. The wavy aerofoils show better lift performance only at higher angles of attacks ($\alpha > 21°$).

The effect of increasing wavelength appears to further slightly delay any stall, with the lift curves of aerofoils 0.5-L and 1-L displaying better lift performance than that of aerofoil 0.25-L, in the post-stall regime of the baseline. Thus, increasing the wavelength of the protuberances decreases the lift performance of the aerofoil at lower angles of attack, within the baseline pre-stall, but has better lift characteristics in the post-stall.

The trend of drag characteristics with increasing wavelength is shown in Figure 15. Increasing the wavelength does not affect the drag coefficient of the wavy aerofoils, as the 3 drag curves essentially lay on top of each other. The baseline aerofoil shows better performance at angles of attack ranging from 0° to 15°, after which its drag curve converges with those of the wavy aerofoils.

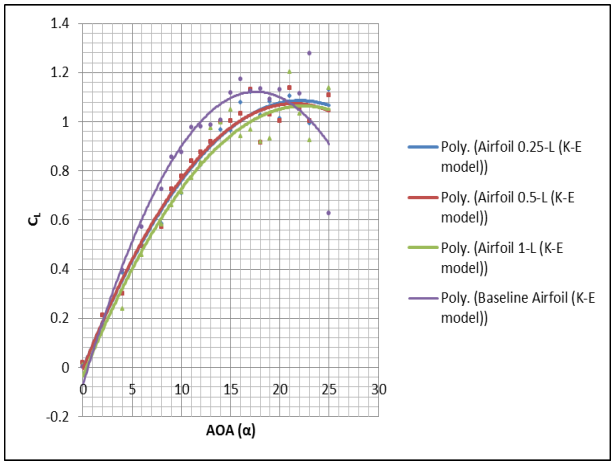

Figure 14: Effect of wavelength on lift (K- ε -model)

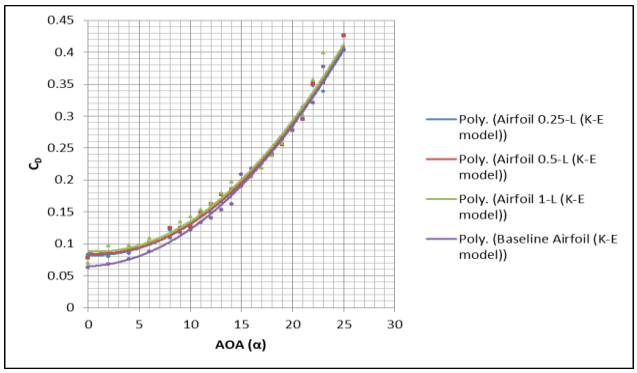

Figure 15: Effect of wavelength on drag

The effect on the lift-to-drag ratio with wavelength variation is shown in Figure 16. As expected, the maximum L/D decreases with increasing wavelength. This is due to the fact that within the baseline pre-stall regime, increasing wavelength has no effect on drag, while slight lift reduction occurs. However, higher L/D is achieved by the aerofoils with increasing wavelength beyond the post-stall of the baseline since at those particular angles of attack; the aerofoils with larger wavelength produce more lift with no drag penalty.

As shown in Figure 18, the presence of protuberances on the aerofoils create flow separation, even at small angle of attack. In the case of aerofoil 0.25-L, as soon as the flow reaches the valleys located behind the leading edge peaks, flow separation occurs. The geometry of the wavy aerofoils is such that increasing the amplitude deepens the valleys. Thus, with deeper valleys, air particles within the boundary layer do not have sufficient energy for attachment to the surface of those valleys. Leading edge peaks have corresponding trailing edge troughs, and thus larger wake patterns are created at the trailing edge troughs which are behind the valleys.

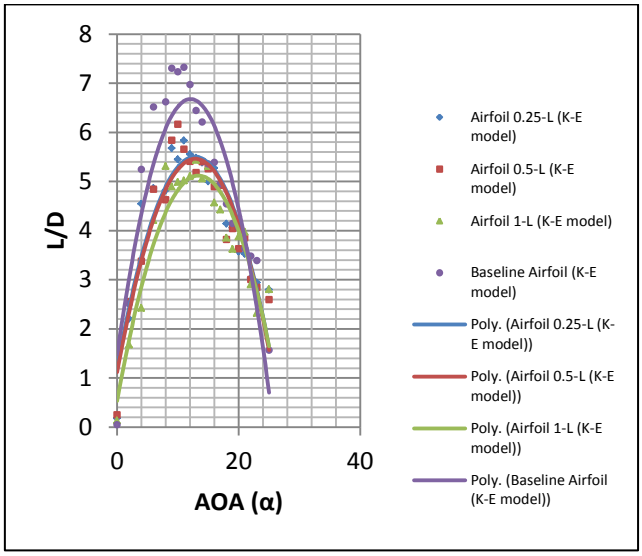

Figure 16: Effect of wavelength on L/D

FLOW ANALYSIS

This part involves investigating the flow behaviour in the pre-stall and post-stall regime of the baseline using the K- ε model.

VARYING AMPLITUDE

Figure 17 shows the surface velocity contour of the baseline aerofoil along those with varying amplitudes when α = 4°.

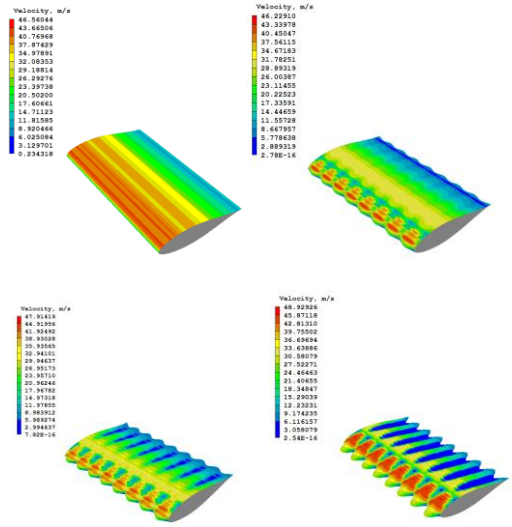

Figure 17: Surface velocity contour α = 4°: (a) baseline, (b) 0.25-S, (c) 0.25-M, (d) 0.25-L

Figure 18 shows the wake patterns at 5mm from both the trailing edges of the baseline and the troughs of aerofoils 0.25-S, 0.25-M and 0.25-L when α = 4°.

As shown if Figure 18, the effect of increasing amplitude leads to the creation of larger wakes at the trailing edge troughs. On the other hand, the baseline aerofoil creates the smallest wake.

The shape of a leading edge protuberance is similar to that of a delta wing which is sharply swept and is known to generate vortices. Figure 19 shows the surface vorticity contours of the baseline as well as those of aerofoils 0.25-S, 0.25-M and 0.25-L.

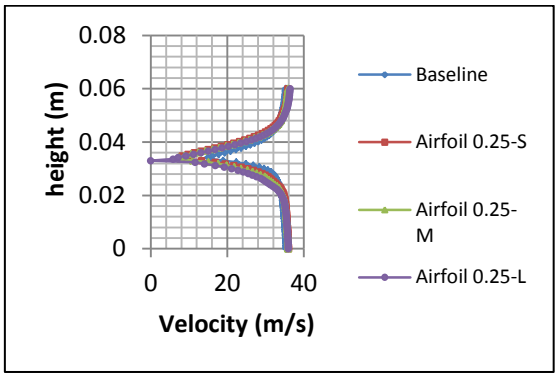

Figure 18: Wake patterns at trailing edge troughs at α = 4° when α = 4°.

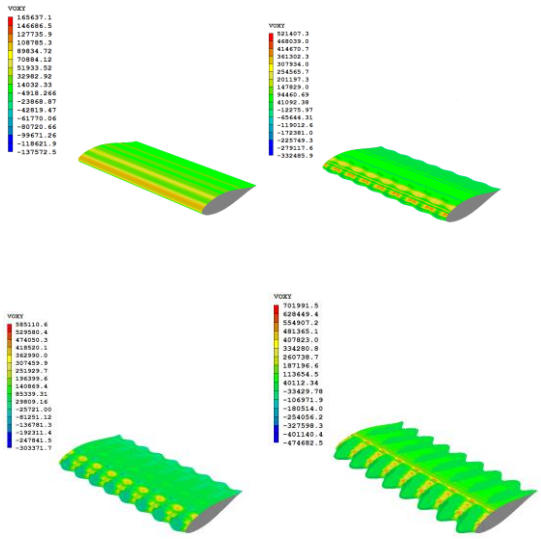

Figure 19: Surface vorticity contour at α = 4°: (a) baseline, (b) 0.25-S, (c) 0.25-M, (d) 0.25-L

Figure 19 confirms the flow visualization experiments performed by Johari et al. (2007), [5], which showed the formation of vortices stemming from leading edge protuberances and migrating towards the troughs of wavy leading edge aerofoils. The strength of the vortices generated by the baseline is negligible compared to those of the wavy aerofoils. It is also determined that increasing the amplitude of the protuberances results in stronger vortices. A leading edge trough has a corresponding trailing edge peak and with increasing amplitude, the stronger vortices within the troughs energize the flow, causing strong reattachment to the surface, thus preventing separation at the trailing edge peaks. This leads to smaller wake patterns at the trailing edge peaks with increasing amplitude, as demonstrated in Figure 20.

Figure 20, shows the wake patterns at 5mm from the trailing edge peaks of aerofoils 0.25-S, 0.25-M and 0.25-L as well as that of the baseline when α = 4°.

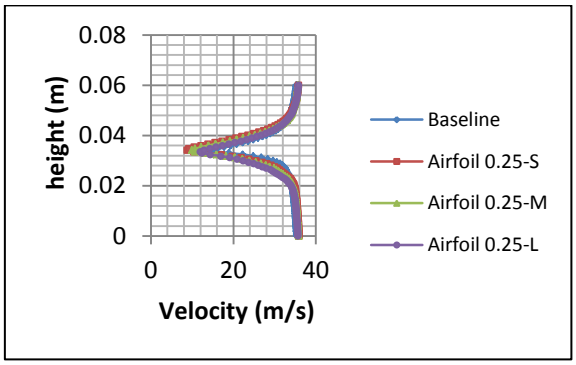

Figure 20: Wake patterns at trailing edge peaks at α = 4°

Varying amplitude as shown in Figure 12, does not affect the drag. This can be explained by the fact that with increasing amplitude, larger wakes produced at the trailing edge troughs are compensated by the smaller wakes at the trailing edge peaks, thus effectively causing the drag to be constant with amplitude variation. The smallest wake is created by the baseline, as opposed to the wakes from both the trailing edge troughs and peaks of the wavy aerofoils, which indicates its better drag performance at α = 4°. The surface vorticity contour of aerofoil 0.25-L at varying angles of attack showed that with an increase in the angle of attack, the vortices created by the leading edge protuberances increase in strength. The lift generated by the baseline aerofoil prior to stalling is only due to the pressure difference, which exists between the lower and upper side of the aerofoil. In the case of the wavy aerofoils, in addition to the pressure difference, lift due to the vortices also occurs. The vortices produced, travel along the side the edges of the protuberances and pull the flow towards the surface of the peaks, preventing separation. At smaller angles of attack, the vortices generated by the wavy aerofoils are weaker leading to a smaller vortex lift which cannot overcome the loss of lift due to the flow separation occurring in the valleys. This explains the lower lift experienced by the wavy aerofoils at low angles of attack. In the post-stall regime of the baseline, the vortices generated are stronger and the vortex lift is able to compensate the loss of lift due to separation, which explains the stall delay characteristics of the wavy aerofoils.

The velocity surface distribution of the baseline along with aerofoils 0.25-S, 0.25-M and 0.25-L when α = 17°, which is prior to the baseline stall, was also obtained (not shown) and indicted that the separated region for the wavy aerofoils is larger when compared to that of the baseline. Increasing amplitude leads to an increase of the separated region. Lift due to pressure difference outweighs the vortex lift experienced by the wavy aerofoils, which explains the higher C_L of the baseline as well as the decrease in the C_L with increasing amplitude. The wake profile comparison of the baseline to those of aerofoils 0.25-S, 0.25-M, and 0.25-L at 5mm from the trailing edge peak and trough when α = 17° indicated that the wavy aerofoils show similar wake profiles at both the trailing edge peaks and trough, which indicates that those aerofoils basically share similar drag

characteristics at $\alpha = 17°$. In sharp contrast to when $\alpha = 4°$, the wake profile of the baseline is similar to that of wavy aerofoils but with a narrower wake. This suggests a smaller separated region causing the drag coefficient of the baseline being only slightly lower than those of the wavy aerofoils. At the higher angle of $\alpha = 25°$, the baseline aerofoil has completely stalled since the flow immediately separates after leaving the leading edge. The wavy aerofoils experience similar flow detachment, but the vortex lift is much higher due to stronger vortices generated by the protuberances and is able to compensate the loss of lift caused by separation. Thus, significantly higher lift is experienced by the wavy aerofoils than the baseline in its post-stall regime, as the flow remains attached to the leading edge protuberances. Increasing the amplitude, leads to a better lift performance at high angles of attack as the peaks have a larger surface area upon which the flow can act upon after being pulled in by the stronger vortices.

VARYING WAVELENGTH

The effect of increasing wavelength essentially diminishes the sharpness of the protuberances and this results in lowering the strength of the vortices generated by the protuberances. As opposed with varying amplitude, which changes the depth of the valleys behind the leading edge peaks, changing the wavelength has no effect on the depth of those valleys. As such similar flow separation occurs in the valleys of aerofoils 0.25-L, 0.5-L and 1-L, which implicates that lift due to pressure differential is the same for all three aerofoils. However, as previously showed in Figure 14, the effect of increasing wavelength leads to a small drop in lift coefficient in the pre-stall regime of the baseline. This can only be attributed to the loss in vortex lift, as weaker vortices are being generated, causing less flow to be attached to the leading edge peaks.

As previously shown in Figure 15, variation in the wavelength does not affect the drag performance. This is further confirmed by the wake patterns of the aerofoils 0.25-L, 0.5-L and 1-L being similar at 5mm from both the trailing edge peaks and troughs when $\alpha = 4°$. The wake pattern at the trailing edge trough, not shown here, shows that a similar flow separation occurs in the valleys irrespective of wavelength. This further confirms that the depth of the valleys play an important role in flow separation. Increasing the wavelength does not offer any advantages within the pre-stall regime of the baseline, as less lift is produced with similar drag. Aerofoils with larger wavelength are more advantageous at higher angles of attack within the post-stall regime of the baseline. Increasing the angle of attack increases the strength of the vortices. Even though weaker vortices are formed with increasing wavelength, they are still strong enough to pull the flow towards the leading edge protuberances, thus creating lift at high angles of attack. A continuous surface area at the leading edge of the aerofoil is occupied by the protuberances, with increasing wavelength. As such, the flow pulled by the vortices act on a larger continuous surface area with increasing protuberance wavelength, thus creating more lift.

CONCLUSIONS

This research investigated the effect of protuberances on both the leading and trailing edge of aerofoil NACA 634-021 on aerodynamic performance. Wind-tunnel testing and numerical analysis using the K- ε model in the PHOENICS software package were conducted to determine the effectiveness of protuberances, as a form of passive flow control. The following conclusions can be drawn from the results obtained both experimentally and numerically:

The standard NACA 634-021 aerofoil perform better at small angles of attack within its pre-stall region, when compared to the wavy aerofoils.

The presence of protuberances on both the leading and trailing edge of an aerofoil is more beneficial at larger angles of attack, delaying stall and having a higher L/D.

The presence of the valleys behind the peaks, leads to flow separation even at small angles of attack. The depth of those valleys is proportional to the protuberance amplitude, with the lower lift being generated by aerofoils with increasing amplitude at lower angles of attack.

Increase in performance at high angles of attack of the wavy aerofoils is due to the formation of the vortices by the leading edge peaks.

Increasing the amplitude of the waviness, lowers performance within the baseline pre-stall regime. Better aerodynamic performance beyond the baseline stall angle is observed with aerofoils having larger protuberance amplitude.

More lift is generated in the post-stall with increasing wavelength, since the flow pulled by the vortices act on an undivided surface area.

The passive form of flow control shown by the protuberances can be appropriate in the application of wings involved in the aerodynamics of high angle of attack, such as fighter jets. For conventional aircrafts, protuberances can potentially be added to the leading edge of the slats, so as to further prevent stall during take-off and landing. Recommendations for future work in this field includes replicating the current study using different aerofoils and parameters, using different type of modelling techniques and performing the simulations at higher Re, more similar to flying conditions.

REFERENCES

[1] Bushnell, D.M. and Moore, K.J. (1991). 'Drag reduction in nature.', Annual Review of Fluid Mechanics 23, Pages 65-79.

[2] Fish, F.M. and Battle, J.M. (1995). 'Hydrodynamic design of the humpback whale flipper.', Journal of Morphology 225, Pages 51-60.

[3] Johari, H., Henoch, C., Custodio, D. and Levshin, A. (2007). 'Effects of leading-edge protuberances on airfoil performance.', AIAA Journal 45 (11), Pages 2634-2642.

[4] Launder, B. E. and Spalding, D. B. (1974). 'The numerical computation of turbulent flows.', Computer Methods in Applied Mechanics and Engineering, 3(2), Pages 269-289.

[5] Miklosevic, D.S., Murray, M.M., Howle L.E. and Fish F.E. (2004). 'Leading edge tubercles delay stall on humpback whale (Megaptera novaeangliae) flippers.', Physics of Fluids 16 (5), Pages 39-42.

[6] Watts, P. and Fish, F.E. (2001). 'The influence of passive, leading edge tubercles on wing performance.', Proceedings of the 12th International Symposium on Unmanned Untethered Submersible Technology, Durham, New Hampshire.